Aalborg Universitet

Boosting battery state of health estimation based on self-supervised learning

Che, Yunhong; Zheng, Yusheng; Sui, Xin; Teodorescu, Remus

Link to publication from Aalborg University

Boosting battery state of health estimation based on self-supervised learning

Yunhong Che, Yusheng Zheng *, Xin Sui, Remus Teodorescu

Department of Energy, Aalborg University, Aalborg 9220, Denmark

ABSTRACT

State of health (SoH) estimation plays a key role in smart battery health prognostic and management. However, poor generalization, lack of labeled data, and unused measurements during aging are still major challenges to accurate SoH estimation. Toward this end, this paper proposes a self-supervised learning framework to boost the performance of battery SoH estimation. Different from traditional data-driven methods which rely on a considerable training dataset obtained from numerous battery cells, the proposed method achieves accurate and robust estimations using limited labeled data. A filter-based data preprocessing technique, which enables the extraction of partial capacity-voltage curves under dynamic charging profiles, is applied at first. Unsupervised learning is then used to learn the aging characteristics from the unlabeled data through an auto-encoder-decoder. The learned network parameters are transferred to the downstream SoH estimation task and are fine-tuned with very few sparsely labeled data, which boosts the performance of the estimation framework. The proposed method has been validated under different battery chemistries, formats, operating conditions, and ambient. The estimation accuracy can be guaranteed by using only three labeled data from the initial 20% life cycles, with overall errors less than 1.14% and error distribution of all testing scenarios maintaining less than 4%, and robustness increases with aging. Comparisons with other pure supervised machine learning methods demonstrate the superiority of the proposed method. This simple and data-efficient estimation framework is promising in real-world applications under a variety of scenarios.

© 2023 The Authors. Science Press and Dalian Institute of Chemical Physics, Chinese Academy of Sciences. Published by ELSEVIER B.V. and Science Press This is an open access article under the CC BY license (http://creativecommons.org/licenses/by/4.0/).

1. Introduction

Lithium-ion batteries are the promising choice of energy storage devices in electric vehicles, portable electronics, and smart grids due to their strengths in high energy and power density, long life span, low self-discharge rate, and high energy efficiency [1,2]. Accurate parameter and state estimations play an indispensable role in battery management systems to ensure safe, efficient, and durable operations [3,4]. State of health (SoH), as a key state describing the health status of batteries, is important to prognostics and health management of battery systems. Therefore, accurate estimation of SoH is beneficial to designing smarter health management strategies and optimizing secondary life usage [5]. Generally, methods for battery SoH estimation can be divided into the model-based and data-driven, where the data-driven method is ever-evolving due to its superiority in accuracy and flexibility

[6,7]. In addition, rapid developments of artificial intelligence, big data, and cloud-edge technologies promote the practical applications of data-driven methods for battery SoH estimations.

Data-driven methods for battery SoH estimation typically consist of four specific steps including data collection and preprocessing, feature extraction and selection, model training, and performance validations [8]. In the first step, the data need to be cleaned to avoid the influence of missing values, abnormal values, etc. on the SoH estimations. The following feature extraction and selection are supposed to extract the aging-related information that promotes the SoH estimation. For feature extraction, many researchers found that the variations of voltage, current, and temperature curves show regular changes along with battery aging processes [9,10]. As a result, some indicators such as variance, entropy, and variational values are calculated as health features [11,12]. In addition, the differential curves also provide profit aging information that can be extracted [13,14]. In addition to features extracted from measured parameters, the physical features can be more valuable for the interpretation of the machine learning

---

* Corresponding author.
  E-mail address: yzhe@energy.aau.dk (Y. Zheng).

models [15]. The extracted features then form a feature matrix, with some features being poorly correlated to battery capacities and others being redundant. Therefore, feature selection should be conducted to determine the optimal feature subset for efficient, accurate, and reliable estimations [16]. In addition to the manual extraction method, the auto-encoder is an automatic way for hidden feature extraction [17]. Another widely used approach is to directly use the data after preprocessing to map the nonlinear relationship between battery SoH in a feature-free manner, such as deep learning methods [18].

The last two steps for data-driven battery SoH estimations are model training and performance validation. For machine learning models, linear regression (LR) can meet the estimation requirement with highly effective features [19]. Nonlinear regression methods such as support vector regression (SVR), gaussian process regression (GPR), and XGboost, show better accuracy and are more robust with different features. In addition, the groups of neural networks are promising ways for data-driven SoH estimation since neural networks are supposed to be able to fit any nonlinear regression tasks [20–22]. One major shortcoming of the conventional machine learning model is being hard to maintain high accuracy and robustness under different testing scenarios, i.e., low generalization ability and robustness. A proper way to handle this problem is to adopt the transfer learning strategy. The main idea of transfer learning is to exploit the knowledge learned in the source domain to improve the model performance in the target domain [23]. Domain adaptation and model parameter fine-tuning are two popular strategies in battery SoH estimation when implementing transfer learning. For domain adaptation, domain discrepancy is reduced by reducing the loss that describes the differences of the hidden features between the source domain and target domain, which helps improve the model accuracy in the target domain [24,25]. Model parameter fine-tuning is aimed to accelerate the convergency on the retraining process in the target domain with a few available labeled data using the model that is pre-trained in the source domain to meet the mapping relationship between the features and SoH in the target domain [26]. However, most of the works with transfer learning are supervised learning, where sufficient labeled data from both the source and the target domain is required. In practical applications, batteries are aged quite differently due to the varieties of battery chemistries, application scenarios, environmental differences, user habits, etc. The acquisition of training data from various batteries is time and labor costing. In this regard, it is of great significance to estimate battery SoH by making use of operational data, including the majority of unlabeled data and very limited labeled data. In this way, the developing SoH estimation method can be time-saving and the estimation method can also be widely applied under different conditions. For model validations, it is supposed to verify and evaluate the performance under different scenarios, e.g., different batteries with different aging conditions, to assess the robustness and generalization of the estimation frameworks, which are not comprehensively considered in most published works.

Therefore, this paper proposes a self-supervised method for the data-driven battery SoH estimation performance boosting. The unlabeled data is used for the pretext learning while sparsely labeled data are used for the downstream SoH estimation model training. The following aspects make this work distinguished from existing research. (1) The self-supervised strategy is proposed for battery SoH estimation with boosted accuracy and robustness. (2) The unlabeled data are used for the pretext training, which eliminates the need for a large labeled training dataset and promotes the downstream SoH estimation. (3) The auto-encoder-decoder is adopted in the pretext learning, and the data preprocessing strategies are proposed, which improves the generalization of the proposed strategy under different charging

profiles. (4) Aging tests with various battery types and operating conditions are conducted to evaluate the accuracy, robustness, and generalization ability of the proposed method.

The remaining parts of this paper are arranged as follows. The experiments and aging datasets are introduced in Section 2. Then, the main methodologies are proposed and described in Section 3, followed by the experimental validation in Section 4. The main conclusions are summarized in Section 5.

2. Experimental

Different aging patterns, which are caused by different battery chemistries and formats and various external conditions, bring big challenges for battery SoH estimations. In this paper, sufficient aging experiments containing different batteries working under different scenarios are conducted to collect data for validation. The testing platform is shown in Fig. 1, where the battery tester, thermal chamber, host computer, and testing batteries are included. The battery tester is used to charge and discharge the batteries during cyclic aging controlled by the host computer. The thermal chamber controls the environmental temperatures where the batteries are placed in. Different battery chemistries, different loading profiles, and different environmental temperatures are considered in the aging test. There are 13 batteries included in the aging experiment, where the battery chemistry and format, loading profiles, and environmental temperature conditions for each battery are listed in Table 1.

The SoH curves of these batteries are shown in Fig. 2, noting that all the capacity values are divided by the first value to calculate the SoH in this paper. Specifically, 6 NCA pouch batteries (with a nominal capacity of 8 A h) are used to simulate the aging under practical electric vehicle applications, where multi-state fast charging (10C–5C–3C–1C) and different discharging profiles are used. During the MCC charging, the battery is charged using the current in the first stage until its voltage reaches the upper limit (i.e., 4.2 V). Then, the current is switched to the second stage to charge the battery to the upper voltage limit again, and this process is repeated until the pre-defined number of charging stages has been accomplished. Afterward, the constant voltage charging is used to continue charging the battery until the current drops below 0.1C. The urban representative profile (UDDS) and highway representative profile (HWFET) are used to simulate the aging pattern under dynamic discharging. In addition to the constant temperature, two batteries are aged under variable temperatures, where the temperatures are changed periodically from the range 25–35–25–15 °C. It is more related to practical applications since the environmental temperatures will change inevitably with weather and seasons. Therefore, the periodic variations of the
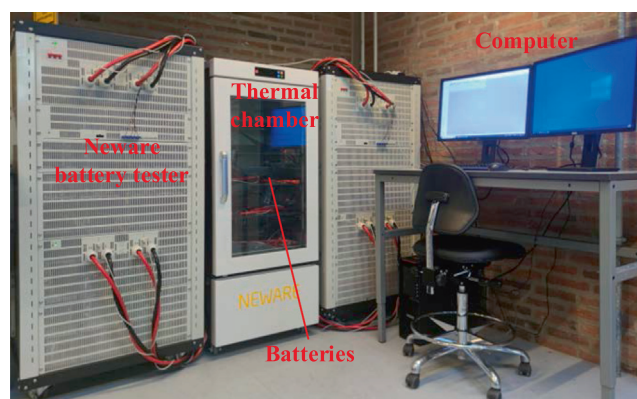

Fig. 1. Platform for battery aging test.

Table 1
Specifications of the experiment data.

Battery	Chemistry	Format	Loading profile (charging-discharging)	Environment temperature
B#1	NCA	Pouch	MCC-CC	25 °C
B#2	NCA	Pouch	MCC-UDDS	25 °C
B#3	NCA	Pouch	MCC-HWFET	25 °C
B#4	NCA	Pouch	MCC-UDDS	25–35–25–15 °C
B#5	NCA	Pouch	MCC-HWFET	25–35–25–15 °C
B#6	NCA	Pouch	CC-CC	25 °C
B#7	NMC + LMO	Prismatic	CC-CC	Room temperature
B#8	NMC + LMO	Prismatic	CC-CC	Room temperature
B#9	LFP	Prismatic	CC-CC	35 °C
B#10	LFP	Prismatic	CC-CC	55 °C
B#11	NMC	Cylindric	CC-CC	35 °C
B#12	NMC	Cylindric	PCC (0.2 Hz)–CC	35 °C
B#13	NMC	Cylindric	PCC (0.05 Hz)–CC	35 °C
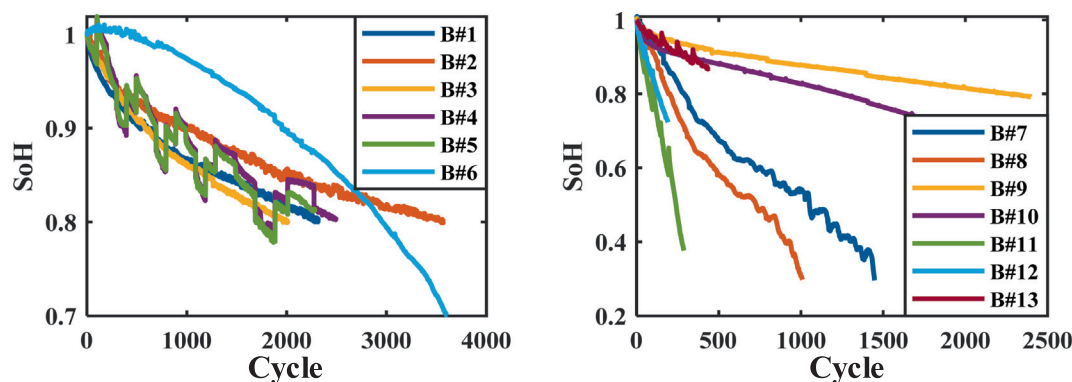
Fig. 2. SoH curves of the 13 aged batteries.

environmental temperatures during our aging experiments help better investigate the battery degradation paths in real-world applications. The first 5 batteries are aged from the fresh condition after manufacture while the sixth (B#6) battery is one retired battery, which is aged under CC charging and CC discharge mode with a current rate of 2.5C. It shows that the aging rate for secondary batteries is higher than those before retirement, indicating more significant aging-related side reactions in their secondary applications. It has also been observed that batteries with highway profiles have faster degradation than those with urban profiles. The possible reason is that the urban profiles have more frequent change in currents, which can reduce the effect of polarization in batteries. Compared to the aging under constant temperature with UDDS profiles, the one under variable temperatures aged faster, though the mean temperature value during operations is the same. It is hypothesized that such a phenomenon is caused by the accelerated solid electrolyte interface (SEI) growth at higher temperatures and lithium plating at lower temperatures with high charging currents.

Other kinds of battery chemistries and formats are also used for aging in this paper. Two prismatic cells (polymer batteries with a nominal capacity of 200 mA h) are aged under CC charging and discharging with 1/3C at room temperature to the SoH reduced less than 0.4. Results show that the inconsistency of manufacturing will cause battery aging at different rates, though the aging conditions are the same. Two NMC prismatic batteries (with a nominal capacity of 100 A h) are aged under 1C CC charging and discharging under 35 °C and 55 °C, respectively. The aging for the B#10 battery is faster than that of the B#9 battery, indicating the higher temperature accelerates the aging though the current loadings are the same. This is because the side reactions such as SEI growth are accelerated with higher temperatures. The last three batteries are

NMC cylindric batteries (with a nominal capacity of 2.2 A h) aged under CC charging/pulse current charging (PCC) and CC discharging under 35 °C. Two frequencies including 0.2 Hz and 0.05 Hz are set for the PCC. These three batteries are discharged under 2C current. The degradation curves show that aging rates under pulse charging currents are lower than that under constant current, which is also consistent with the lower aging rates using UDDS profiles mentioned before since pulses reduce the effects of polarization that cause battery aging.

It can be seen from the descriptions and the information in Table 1 that the aging scenarios included in this paper are various, providing data from different aging patterns. Therefore, the SoH estimation method presented below can be evaluated more comprehensively under different batteries and different aging patterns, making the verification more general and convincing. The SoH curves show that different batteries are degraded in different ways, which causes the SoH to have different degradation patterns and various degradation rates. The first five batteries show the sublinear shapes during their primarily used span, where variable temperatures cause the degradation curves to be stage shaped. B#6 is a retired battery that shows a super-linear shape, which means the whole degradation rate of this kind of battery is in accelerating-stable-accelerating mode. The other kinds of batteries with other charging-discharging modes and environmental temperatures all show stable degradation rates entire the whole aging process. Overall, these various aging data help conduct more comprehensive evaluations of the estimation methods.

3. Methodology

Self-supervised learning is a novel learning strategy developed rapidly in recent years, which aims to benefit the downstream task

via learning that leverages input data itself as supervision [27]. To achieve this goal, a pretext task and the target task are usually used for the representation learning and the downstream application [28]. In battery SoH estimation with a self-supervised learning strategy, the feature representative task and the downstream SoH estimation task are defined for the two main tasks respectively, which are introduced in detail below.

3.1. Self-supervised learning for battery SoH estimation

The overall framework of the proposed self-supervised learning strategy for boosting battery SoH estimation is shown in Fig. 3. Specifically, four main steps are included, which are data preprocessing, pretext task pre-training, downstream target task fine-tuning, validation and evaluation under different scenarios. In the data preprocessing, different aging data collected from different batteries with different chemistries and formats aged under different loading profiles and environmental temperatures are filtered and aligned for the following modeling or testing. Unlabeled data and sparsely labeled data are included for use in pretext learning and downstream target learning respectively. Then, pretext learning aims to learn the aging characteristics hidden in the partial capacity-voltage (*Q-V*) curve via unsupervised learning where the auto-encoder-decoder is adopted for feature learning. After that, the encoding part of the pretext-trained network is transferred to the downstream target network and an output layer is added. The sparsely labeled data are then used for fine-tuning to map the relationship between the partial capacity-voltage curve and battery SoH. Finally, the model is used for the SoH estimation

where different testing scenarios are considered to evaluate the accuracy and robustness. The detailed process of each step in Fig. 3 is described in the following subsections.

3.2. Data preprocessing

As introduced before, data preprocessing is the first and one important step in the data-driven battery SoH estimation which significantly influences the performance of the estimation models. In this paper, the charging capacity and voltage data that can be measured online by the battery management system are used as known information for SoH estimation. A voltage range during the charging process is first selected. The corresponding capacity during this voltage range can be calculated by the ampere-hour counting method,

$$Q = \int_{t=0}^{N} I dt \tag{1}$$

Then an interval voltage (5 mV in this paper) is used to segment the voltage range, and the interpolation method is used to obtain the capacity segments based on the measured *Q-V* curve. The length of the *Q-V* curve keeps the same during the whole aging process in this way. In this paper, the voltage range is selected as [3.3 V, 3.5 V] for LFP batteries, [3.8, 4.1] for NMC cylindric batteries, [3.6, 4.2] for the fast-charging NCA batteries under their first stage charging process in MCC and NMC + LCO batteries. These voltage ranges are selected via trials by considering the real-world applications where batteries typically undergo partial charging instead of full charging.
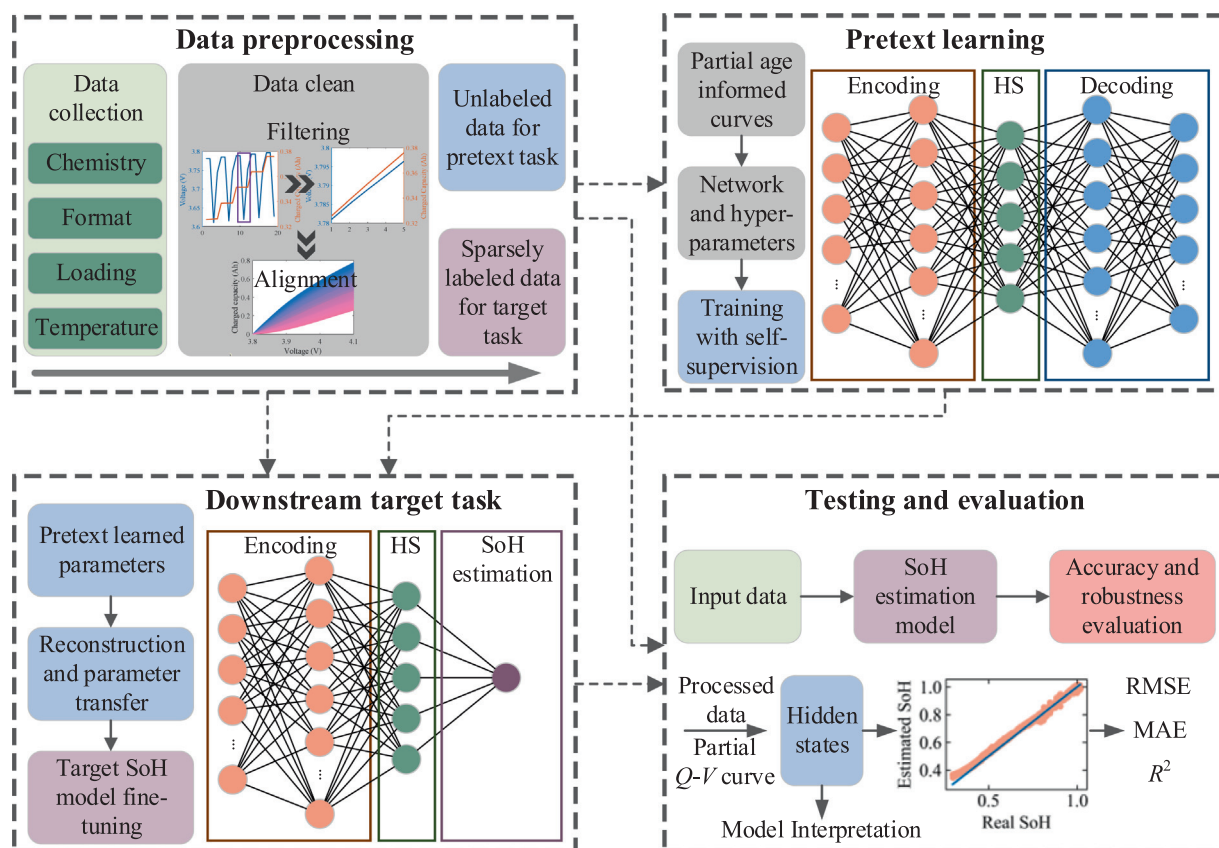

Fig. 3. Overall framework for the self-supervised battery SoH estimation.

Fig. 3. Overall framework for the self-supervised battery SoH estimation.

For the pulse charging mode, the voltage show fluctuations since the current is in 'on-off' modes. Therefore, filtering is required first to smooth the curve. Instead of using a filter to smooth the original curve directly (such as the Gaussian filter or moving average filter), which may change the shapes and cause information loss, we remove the rest period during the pulse charging to make the charging curve smooth. The idea and effectiveness of the processing method are illustrated in Fig. 4(a and b). Since the capacity keeps unchanged although the voltage goes down during the rest period in the pulsed current charging process, the data corresponding to the rest period can be removed, so that the capacity curve increases monotonously. The voltage increases when loading the current again after rest, while it may not change too fast to become larger than the voltage value before the rest at the following several samples. Therefore, to ensure the voltage curve change monotonously, the period when the voltage is still lower than the value before the rest is also removed. Finally, after the data alignment, a monotonous *Q-V* curve is obtained, as shown in Fig. 4(d), which has large fluctuations of the raw parameters as shown in Fig. 4(c). The interpolation method could be then applied to prepare the inputs for the data-driven model on this processed *Q-V* curve. The proposed data clean method under pulse current has several benefits. Firstly, the main aging information contained in the charging process remained properly while the smoothed data can be used for data alignment. In addition, the processing method is suitable for wide pulse current scenarios with different frequencies and duty cycles. Furthermore, this filtering method can also be used in the multi-step charging for the filtering during the current switch stages. Therefore, the data preparation for the data-driven modeling is general for different charging modes. The processed data are used for the modeling in pretext learning and target task learning without or with labels respectively, which are described in the following subsections.

3.3. Feature representative self-learning

Most of the data collected in practical applications are unlabeled, which is ignored by most conventional data-driven methods since no labels can be used for supervised learning. However, the aging information hidden in the operating data such as voltage and charged capacity curves has a high correlation with battery aging that can be used to boost the accuracy of the SoH estimation model. Therefore, in the feature-representative self-learning process, the unlabeled data is used to learn the hidden relationship between the processing data and battery aging, which is the pretext task in self-supervised learning. The partial charging capacity-voltage curve is selected as the input information while an auto-encoder-decoder structure is adopted to learn the hidden aging features.

Specifically, the historical data of the charged *Q-V* curves after data cleaning using the method described above during each cycle is input for the encoder-decoder structure. After encoding the information, the decoding part is used to reproduce the charged *Q-V* curves, where the reconstructed curve and the original curve are used to calculate the mean square error as the loss to be reduced during training,

$$\mathrm{MSE} = \frac{1}{n} \sum_{i=1}^{n} (y_i - \widehat{y}_i)^2 \tag{2}$$

where y_i and $\hat{y}_i$ are the measured curve and reconstructed curve respectively. The $\hat{y}_i$ is output sequence of the encoder-decoder structure. The neurons of the first and second encoding layers are set as 50 and 25 respectively, which are reversely set for the decoding layers. The hidden features that are used to represent the aging characteristics are set as 5, meaning that the neuron number of the
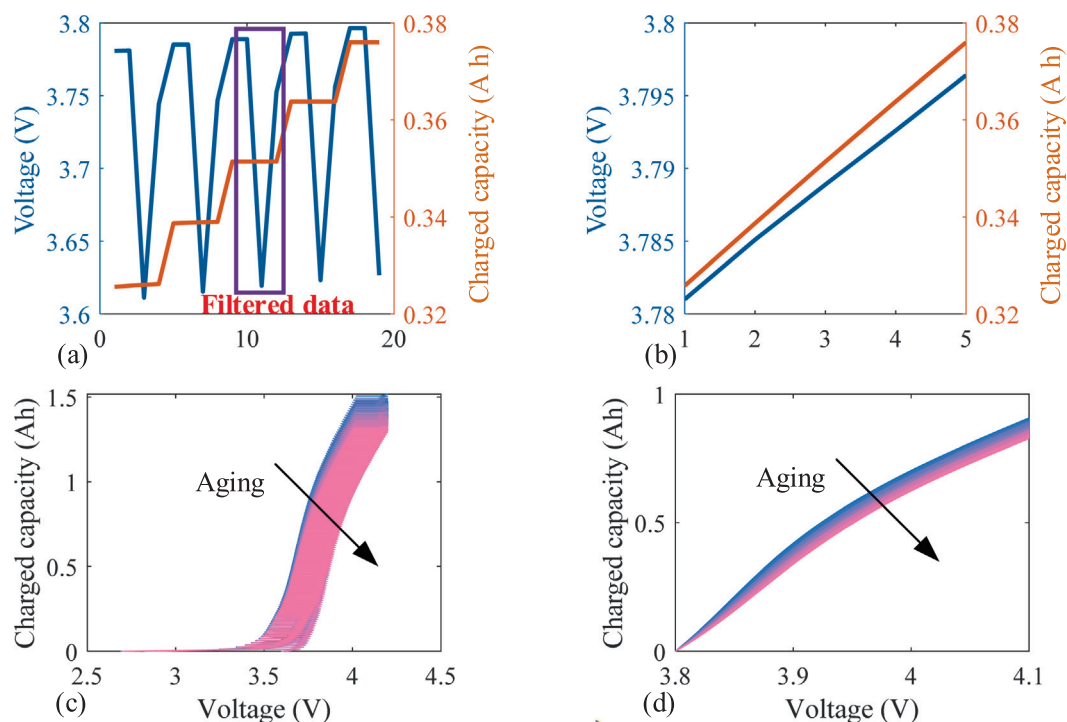
Fig. 4. Demonstration of the proposed data alignment method. (a) Original voltage and charged capacity curves and illustration of filtering location. (b) Voltage and charged capacity after data cleaning. (c) Original Q-V curves during aging. (d) Cleaned Q-V curves during aging.

middle layer is set as 5. The setting of the neurons is conducted by trialing with the aim to keep it simple while ensuring performance.

The interpretability of the machine learning-based method is one significant objective to know the reason for such performance while most of the previous works ignored. Generally, model-based methods and post hoc methods are popular for machine learning model interpretation [29]. In this paper, we adopt the post hoc analysis with the correlations between the hidden states after auto-encoding are used to interpolate the effectiveness of the pretext learning. Pearson correlation coefficient is one popular index for the correlation evaluation between features and battery capacity. The expression of the Pearson correlation coefficient to present the correlation between two variables x and y is shown as follows [26,30],

$$\rho = \frac{\sum_{i=1}^{n}(x_i - \bar{x})(y_i - \bar{y})}{\sqrt{\sum_{i=1}^{n}(x_i - \bar{x})^2}\sqrt{\sum_{i=1}^{n}(y_i - \bar{y})^2}} \tag{3}$$

The unlabeled data are used to train the encoder-decoder network and then the pre-trained encoder network is used for the downstream SoH estimation model fine-tuning, which is introduced below.

3.4. Downstream SoH estimation learning

In practical applications, only sparsely limited labeled data could be obtained while most of the data are unlabeled, which have been used to the pretext task learning above. Then, the downstream target task is to fine-tune the network by several sparsely labeled data through supervised learning. The encoding layers are adapted with one output layer for the final SoH output, and the number of neurons in this layer is set as 1. Therefore, the output for the fine-tuning is the sparse labeled SoH. The input data is also the partial Q-V curve, which has the same format as the pretext learning while only the Q-V curves of the cycle with sparse labeled SoH are required. After the fine-tuning process, the final network for battery SoH estimation is verified and evaluated through the testing data. The previously learned information through the unlabeled data maintains in the encoding layer while the new regression relationship is rapidly learned through the slightly fine-tuning process. Therefore, the self-supervised learning strategy helps increase the aging information that the neural network learned while accelerating the convergency process during downstream target task training. Compared to existing transfer learning-based battery SoH estimations, the proposed method transfers the learned information from unlabeled samples without the need for sufficient samples from the source domain. Therefore, the proposed method is more efficient with only limited labeled samples. The model is developed in Python using Pytorch in this paper. The learning rate is set as 10^{-3} while the epoch is set as 5000 to let the neural network be well trained.

4. Results and discussion

To evaluate the performance of the proposed method, several experiment aging tests with different batteries are conducted to produce data for validation under different aging scenarios. The root-mean-square error (RMSE), mean absolute error (MAE), and R square (R^2) between the estimated SoH and the ground truth are calculated for the accuracy evaluation. The expressions of these three indexes are as follows,

$$RMSE = \sqrt{\frac{1}{N}\sum_{i=1}^{N}(y_i - z_i)^2}, \tag{4}$$

$$MAE = \frac{1}{N}\sum_{i=1}^{N}|y_i - z_i|, \tag{5}$$

$$R^2 = 1 - \frac{\sum_i(y_i - z_i)^2}{\sum_i(y_i - \hat{y}_i)^2}, \tag{6}$$

where y represents the true value and z is the estimated value while $\hat{y}$ is the mean value of all the true values. It means better estimations with lower RMSE and MAE while higher R^2.

4.1. Pretext learning evaluation

The encoding process is mainly aimed to learn the aging information hidden behind the unlabeled data. To evaluate the performance of the pretext learning, the correlations between the learned hidden states and battery capacity are evaluated. The variations of the hidden features against battery capacities of B#1 are shown in Fig. 5. The correlation analysis results between each hidden state (HS in the figure) and battery capacities for B#1 and numerical results for all 13 testing batteries are presented. It shows that all the five encoded hidden states have high linear relationships with the battery capacities, which means that the autoencoder extracts the key aging information satisfactorily. In addition, it also provides the proper interpretation of the downstream SoH estimation model that high correlations exist between the hidden states and the final output (SoH) of the machine learning model.

The numerical results for all 13 batteries illustrate that the pretext learning for the aging characteristic information extraction is suitable for different batteries working under different scenarios. Most of the Pearson correlation coefficients are larger than 0.99. The correlation coefficients under variable temperatures and high temperatures are lower than that under normal temperatures, indicating that the temperature variations influence the learning performance of the pretext task. The correlation coefficients also reduce under pulse charging profiles but not significantly, which proves that our data preprocessing method maintains the main aging information and suits different application requirements. The statistical results are listed in Table 2. Larger mean and minimum values are assumed to be better, while smaller interquartile ranges are assumed to be better. The mean values for the five hidden states are larger than 0.96 and the minimum values are larger than 0.87. The interquartile range is small for all five hidden states (less than 0.012), which means the pretext learning is robust under different application scenarios. Therefore, the pretext learning using unlabeled data helps learn the aging characteristics satisfactorily, which helps the performance of the downstream target task learning for battery SoH estimation that is demonstrated in the following section.

4.2. SoH estimation

The pretext learning performance demonstrated above shows that the main aging information is learned through the auto-encoder using the unlabeled data. Then, the downstream SoH estimation for batteries aged under different conditions is presented and evaluated in this section. The pretext learned parameters of the neural network are transferred to the target task while a few labeled data are used for the final fine-tuning for SoH estimation. Firstly, the firstly 20% of the data are used for pretext learning while only three labeled data (first cycle, the point at 10% of the data, point at 20% of the data) are used for the downstream fine-tuning. The estimation results for each battery cell, estimations and estimated error distribution density of all the batteries are shown in Fig. 6. The numerical results are listed in Table 3. It shows
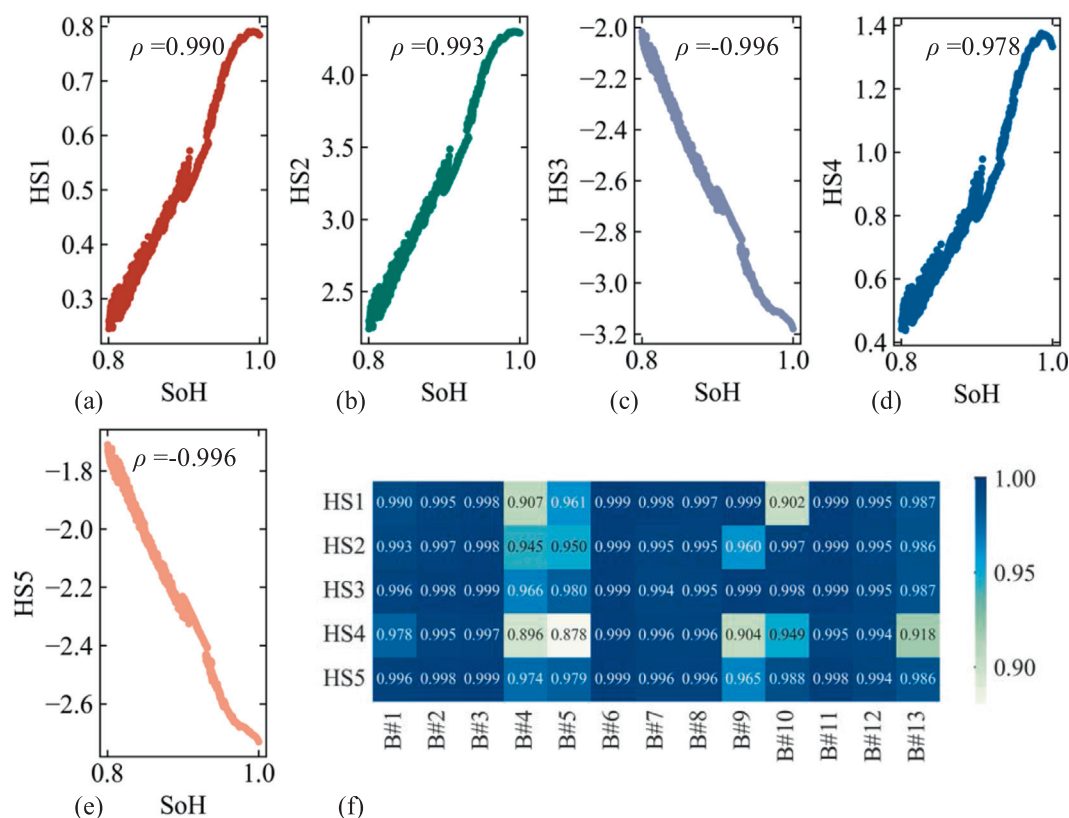
Fig. 5. Correlation evaluations between the five encoded hidden states and battery capacities, (a–e) exemplary results for B#1 and (f) results for all 13 batteries.

Table 2
Statistic results of the correlation evaluation.

Hidden state	Mean	Minimum	Interquartile range
HS1	0.979	0.901	0.011
HS2	0.985	0.945	0.108
HS3	0.993	0.966	0.005
HS4	0.961	0.878	0.078
HS5	0.990	0.965	0.012

that the estimated values fit the real values satisfactorily for all 13 batteries regardless of different battery types, working scenarios, and environmental temperature conditions, indicating the generalization and robustness of the estimation method and the effectiveness of the pretext aging characteristic learning. As for the estimations of each specific scenario, a detailed evaluation is presented below.

For the NCA batteries (B#1 to B#6), estimations are more accurate for the primarily used batteries even with dynamic discharging profiles. For the estimations of the two batteries working under variable temperatures, the estimated values show larger distances to the real values but still converge satisfactorily to the real values, which means the estimations under variable temperatures and different aging profiles are robust. The estimations for the second-life battery, which has a different degradation curve shape are still accurate, indicating the model support estimations for batteries during both primary life and secondary life. The RMSE and MAE for these 6 batteries are less than 1.28% and 1.14% respectively with R^2 larger than 0.95.

For the polymer batteries working under room temperature for the whole life span (SoH drops below 0.4), the results showed in Fig. 6(g and h) also show satisfactory estimations with RMSE and

MAE less than 3% and 2.9% and R^2 larger than 0.96. There are some large fluctuations caused by capacity recovery, as the capacity curve shows in Fig. 1. It shows that the errors are larger for these two batteries since a wider life span and long-running cycles are included. For the LFP batteries (B#9 and B#10) working under high temperatures with CC, the results are accurate with smaller errors.

The last kind of battery (NCM batteries) is aged under both CC charging and pulse current charging. The data preprocessing and estimation method also support the SoH estimations under pulse charging profiles, which extend the application capability. The estimation results show that some outliers exist but most of them are well-fitted to the real values. The RMSE, MAE, and R^2 are 0.873%, 0.615%, and 0.987 for the battery charged with 0.2 Hz, and those are 0.645%, 0.425%, and 0.965 for the battery charged with 0.05 Hz.

The estimation results for all the batteries are shown in Fig. 6(n) and the distribution of the errors is shown in Fig. 6(o). It shows that all the absolute values of the errors are less than 5% and most of them are less than 2%. Therefore, the SoH estimation is robust and accurate under different application scenarios for different battery chemistries and formats, which is promising for practical applications since only own unlabeled information and a few labeled data are needed.

The robustness of the method with different ratios of data that are available for self-supervised learning is evaluated then. The labeled data for the downstream target task are several points at each 10% of the entire cycle number for each battery. The variations of RMSE, MAE, and R^2 with different ratios of data for modeling are shown in Fig. 7. The results indicate that the errors sharply reduced to lower ranges while R^2 increase quickly to higher values from 10% to 20%, and then keep stable with later ratios and an overall improvement trend until 90%. Some outliers exist with ratios less than 50% and disappear after that, which means the
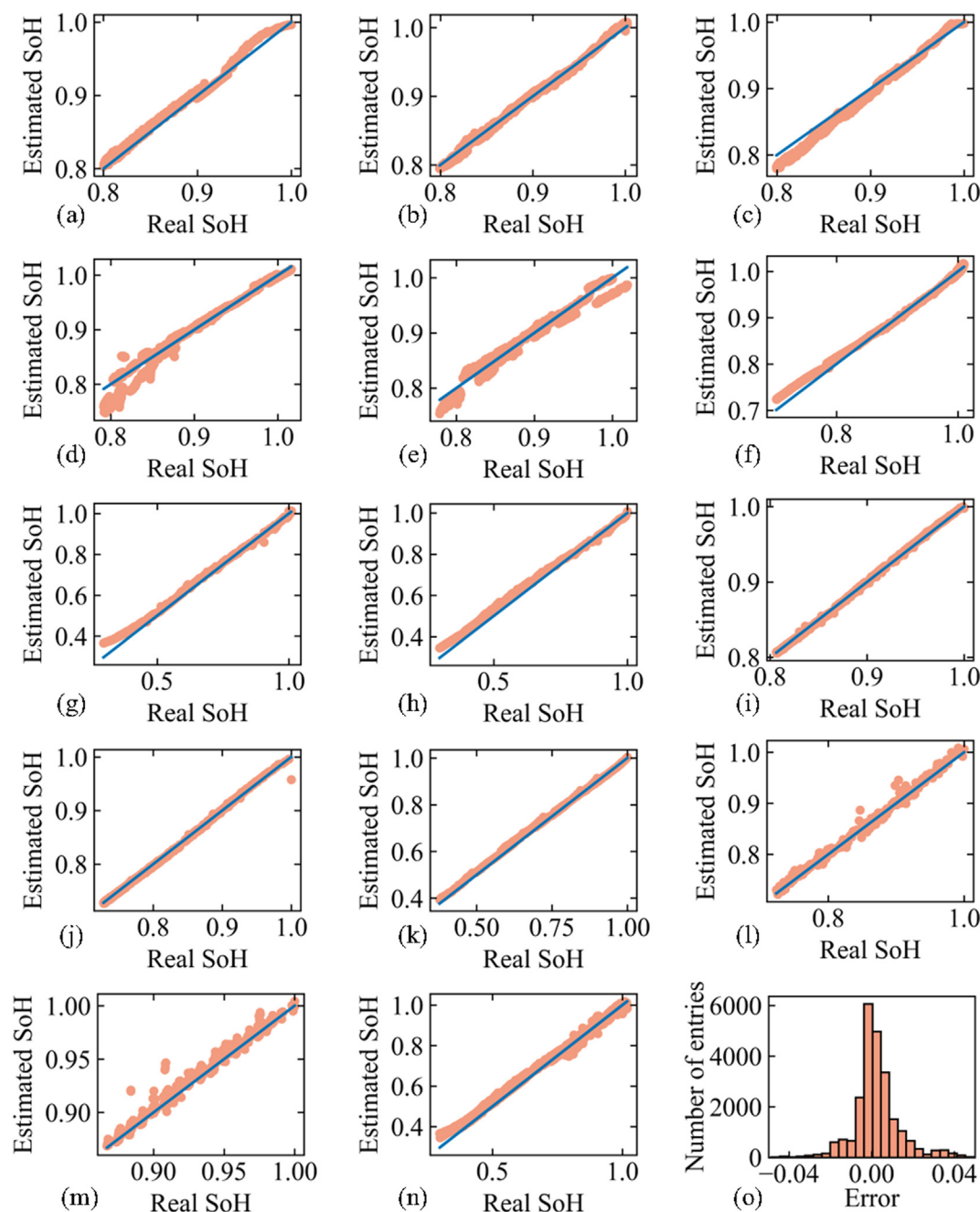
Fig. 6. SoH estimation results. (a–m) for B#1-B#13, (n) for all the batteries, and (o) errors distribution density for all the batteries.

Table 3
Numerical results for the SoH estimations.

Battery	RMSE (%)	MAE (%)	R^2
B#1	0.712	0.658	0.977
B#2	0.382	0.314	0.995
B#3	1.272	1.134	0.956
B#4	1.276	0.860	0.954
B#5	1.141	0.930	0.957
B#6	0.883	0.638	0.988
B#7	2.067	1.762	0.984
B#8	2.968	2.673	0.967
B#9	0.169	0.146	0.999
B#10	0.282	0.227	0.998
B#11	1.235	1.060	0.994
B#12	0.873	0.615	0.987
B#13	0.645	0.425	0.965
All	1.139	0.762	0.989

overall robustness and accuracy are continually improved. It shows from Table 3 that only with 20% of data (only three labeled samples), the errors are less than 3% while R^2 is larger than 0.95, indicating satisfactory estimations. Therefore, the proposed method achieves satisfactory estimation performance with only early data for modeling and can be continually improved for more robust and reliable estimations along with the usage of unlabeled data and several labeled samples.

Then, mutual verification is conducted to further evaluate the proposed framework, where the batteries of B#1-B#3 are used for pretext learning using the partial Q-V curve without labels. Then, the downstream fine-tuning is conducted with the early sparsely labeled samples (three points from the first 20% of data), where the results for B#4-B#7 are shown in Fig. 8(a–d) respectively. The testing scenarios of Fig. 8(a and b) are used to

evaluate the information from the constant temperature on the performance improvement under variable temperatures. Results in Fig. 8(c) can be used to verify the effects that aging information
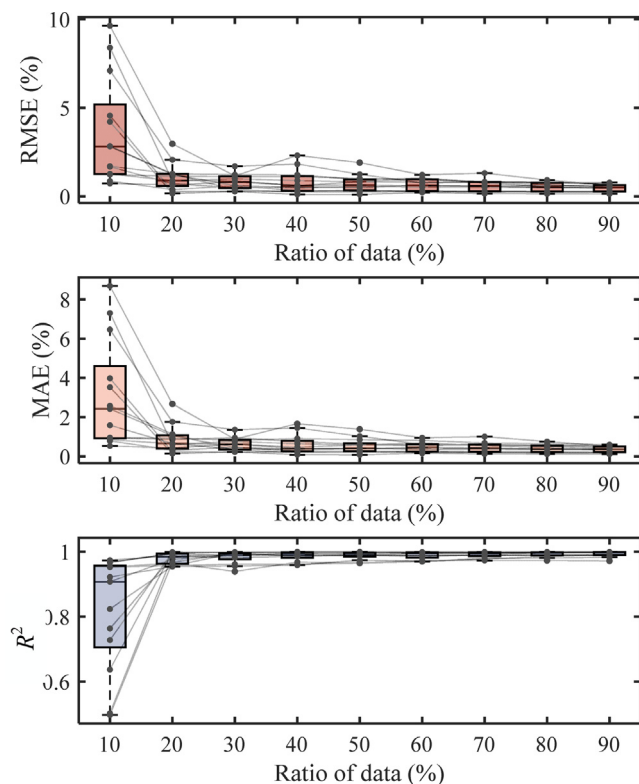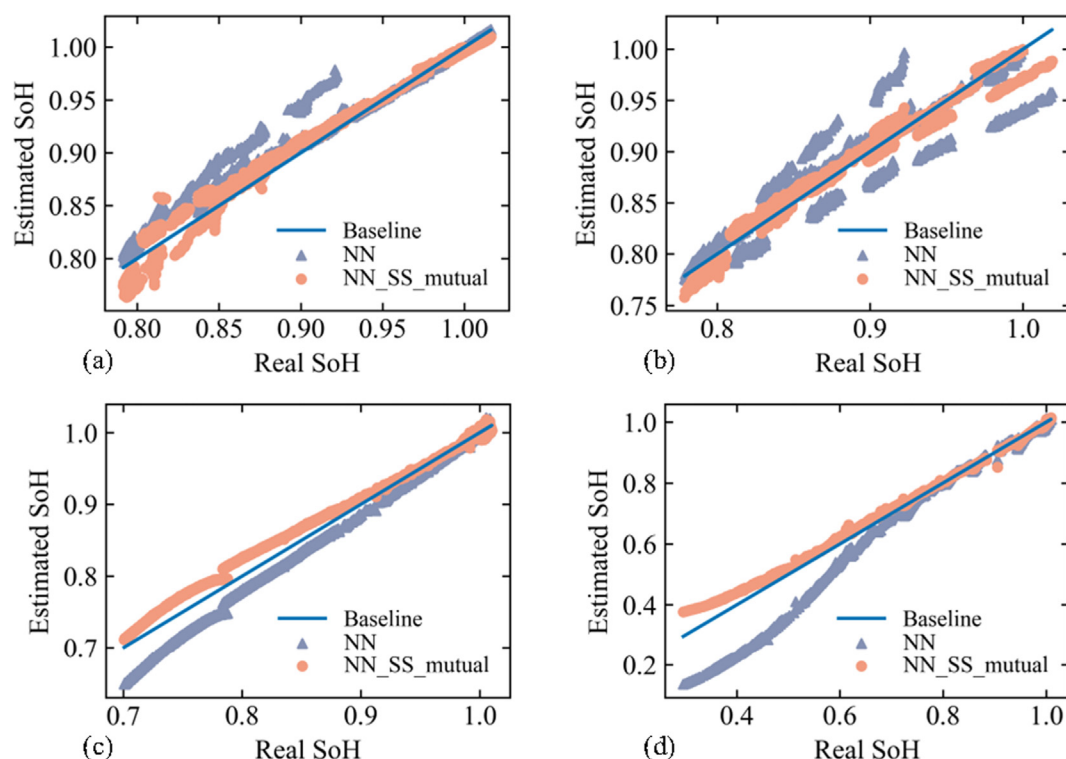
learned from fresh batteries is beneficial for the accuracy improvement of the secondary battery. The last testing scenario in Fig. 8(d) is aimed to prove that the aging information from one kind of battery is also useful for SoH estimation of the other kind of battery. These test scenarios also have practical significance. It is challenging for model training with a large number of samples for the onboard battery management system. It is valuable to use the pretext model trained by using data from other batteries while only using sparsely labeled data for the downstream fine-tuning for performance improvement. Therefore, the proposed framework is also effective in mutual usage.

4.3. Comparative evaluations

In order to demonstrate the advantage of the proposed SoH estimation framework, results obtained by several conventional methods are presented and compared. Firstly, four representative batteries (B#4, B#6, B#7, and B#13) are used for the demonstration and the estimation results based on different methods are shown in Fig. 9. Both primary and secondary life batteries, both dynamic loading profiles, pulse currents, and constant current loading profiles, both constant and variable temperatures are represented by these four batteries. The NN without self-supervised learning, LR, GPR, ridge kernel regression (Ridge), random forest regression (RF), k-nearest neighbors (KNN) regression, and SVR are included for the comparisons. Therefore, both kernel-based and parameter-based machine learning algorithms are considered for the evaluations. The inputs of these models are the preprocessed partial Q-V curve. Only the labeled data are used for the supervised learning requirement. The symbol 'NN_SS' is the result obtained by the proposed method in this paper. It shows that our model has the best generalization capability, with high accuracy under different testing scenarios. In contrast, other conventional machine learning methods such as RF and KNN failed to map the

Fig. 7. Evaluations of the estimation performance with different ratios of data available for modeling.

Fig. 8. Performance of the proposed method with unlabeled information from other batteries. (a) Results for B#4, (b) results for B#5, (c) results for B#6, and (d) results for B#7.
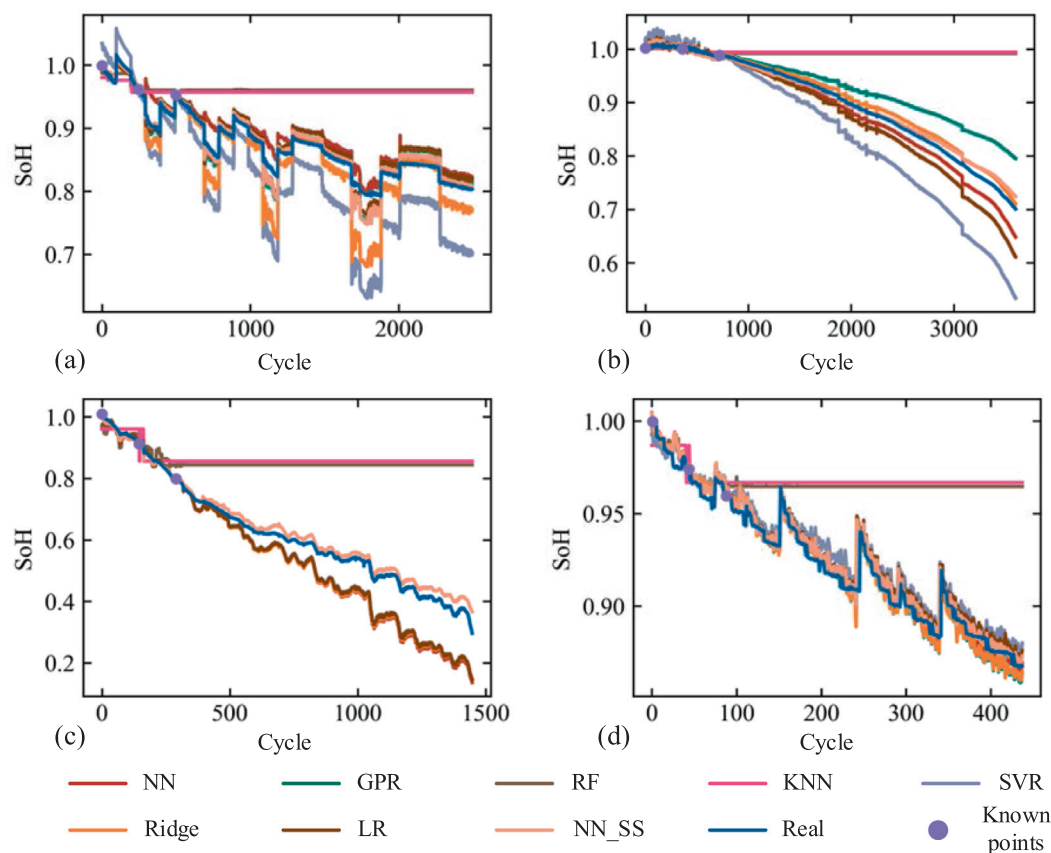
Fig. 9. SoH estimation results with different methods for (a) B#4, (b) B#6, (c) B#7, and (d) B#13.

relationship due to the limited labels, showing worse robustness and generalization. The reason for the poor performance of conventional machine learning methods in our case is that they require sufficient labeled data for training, which are very difficult to be obtained in real-world applications. Therefore, the proposed method in this paper is a more efficient way for battery SoH estimation with limited labeled samples since many unlabeled samples can also be leveraged to provide knowledge of battery degradation.

To evaluate the performance more clearly, the numerical comparisons are shown in Fig. 10 and the numerical results are listed in Table 4. Each dot in the figure represents the result for one battery cell using the corresponding method while the distribution represents the robustness and generalization of each method on different application scenarios. It shows that from Eq. (6) that R^2 can be negative values. When R^2 is lower than 0, we set it as 0 since the small negative value will influence the clear illustration of Fig. 10. Also, these values can be seen as poor estimations that indicate poor generalization. The numerical results listed in Table 4 are the average values of each index based on the results of all 13 batteries, which demonstrates the average performance of each kind of method under different application scenarios. Fig. 10 shows that conventional machine learning models with supervised learning have large error distributions. While the proposed method with the self-supervised learning strategy has the smallest error distribution, where all the errors are in a lower range and the R^2 is in a higher range. From the numerical results in Table 4, where the mean value of each index in Fig. 10 with each method is listed, the improvement of the accuracy can be better illustrated. The average RMSE and MAE are only 1.07% and 0.88% while those of the conventional methods are larger than 2.27% and 1.73% respec-

tively, which means the proposed method can reduce the error more than 1 time. The average R^2 is 0.978 for the NN_SS which is also larger than the other methods, indicating better convergency to the real values. The average maximum absolute error is only 3.336%, which means that the estimations maintain a narrow error range, indicating better reliable estimations compared to other methods. Therefore, from the comparative evaluations above, the proposed method successfully improves the accuracy and robustness of battery SoH estimation by the self-supervised learning strategy.

4.4. Discussion

The proposed method has been evaluated above for performance improvement in battery SoH estimation, where both self-verification and mutual verification have been conducted. Different conventional machine learning models are also used for the comparisons. To further demonstrate the effectiveness of the proposed framework, a public dataset from [31] is used for verification, where "Dataset 2" with NCM batteries is used. The results are shown in Fig. 11, where the histograms of the RMSE and MAE for all the batteries are illustrated. The pretext training the downstream fine-tuning also uses the first 20% unlabeled data and three sparse labeled data, respectively. The results show that both the RMSE and MAE shift to the lower values with the proposed framework, which means the accuracy is improved by learning from the unlabeled samples. Based on both the experiment data and public data, the proposed framework is verified to be effective in battery SoH estimation performance improvement in different working conditions with different battery types.
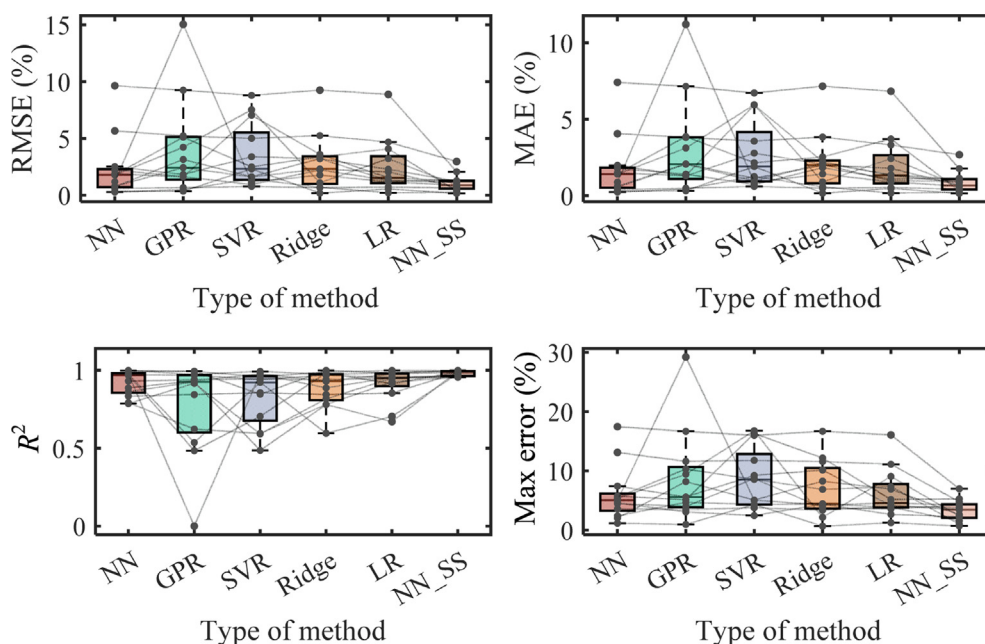
Fig. 10. Evaluations of the estimation performance with different models.

Table 4
Mean values of each index for different methods.

Method	RMSE	MAE	R^2	Max error
NN	2.268	1.730	0.921	5.997
GPR	3.928	2.961	0.779	8.645
SVR	3.391	2.653	0.830	8.645
Ridge	2.840	2.094	0.883	6.828
LR	2.464	1.909	0.909	6.140
NN_SS	1.070	0.880	0.978	3.336

From the results presented and evaluated above, the proposed method has superiority for accuracy and robustness improvement by taking advantage of unlabeled data besides the labeled data. The unlabeled data are valuable for aging characteristics learning while being ignored by most of the previous works. In order to demonstrate the performance of the proposed method, an interval of each 10% of data is used to assume the availability of labeled samples. In real applications, this can be different due to the practical scenarios. For example, the labeled data can be obtained during regular maintenance while sufficient unlabeled data are available in most daily charging processes. The performances under different charg-

ing profiles have been verified. Therefore, the proposed method can be easily transferred to practical applications by using sufficient unlabeled data and a few sparsely labeled data. Compared to existing transfer-learning methods, which require sufficient labeled data from the source domain, the proposed method can estimate battery SoH accurately without information obtained from other batteries while taking advantage of historical unlabeled data for performance improvement. In addition, the feedforward neural network is used for the verification of the proposed estimation framework considering the simplicity and low training burden. Other advanced deep neural networks that have been used for battery SoH estimation, such as long-short-term memory [20,25], gated recurrent units, and convolutional neural networks [32], can also be implemented by adopting the proposed framework. Therefore, the generalization of the proposed method is high for different practical applications. Furthermore, it is valuable to investigate the performance under different partial charging depths, i.e., different voltage ranges. It has been investigated that different voltage ranges for battery impedance prediction are effective by considering physical interpretations [33]. In our future work, the performance of battery health estimation and prognostics with different voltage ranges will be investigated, and the physical correlations will be also studied.
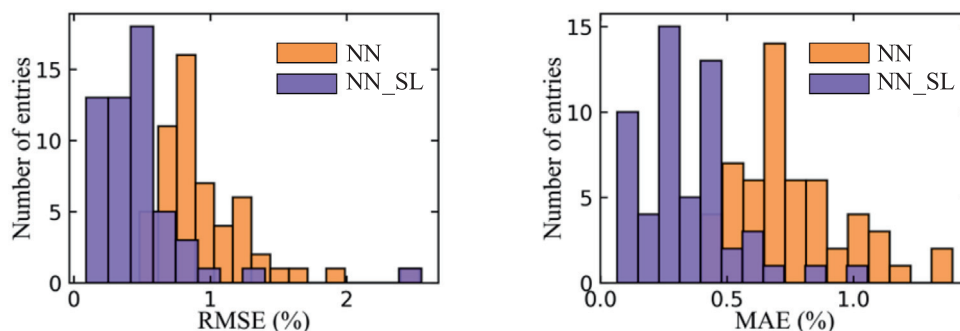

Fig. 11. Evaluations of the estimation performance using a public dataset from [31].

5. Conclusions

Battery SoH estimation is one key function in battery management systems for efficient health management. However, conventional data-driven methods require sufficient labeled data for modeling, which hinders practical applications. This paper proposed a novel self-supervised method to boost the battery SoH estimation by introducing a pretext aging characteristic learning with unlabeled data and a downstream target task learning with a few labeled data. A filter-based data preprocessing method is proposed to ensure the smooth partial capacity-voltage curves obtained under different charging modes. The auto-encoder-decoder is used in pretext learning for hidden feature extraction. Pearson correlation analysis indicates that the average coefficients between the learned hidden features and battery SoH are larger than 0.96, which proves the efficiency of the learned aging characteristics. With only a few labeled data used for the downstream SoH estimation task learning, the accuracy and robustness of the proposed method are proved to be improved compared to conventional machine learning methods. With only three labeled samples, the average RMSE and MAE are 1.07% and 0.88% respectively with the mean maximum absolute error of 3.336%. The fitting coefficient R^2 is 0.978. Verifications are conducted under different batteries with different loading profiles and temperature conditions. The robustness of the method can be continually improved along with its usage during aging. In future work, the future trajectory prediction with self-supervised learning will be studied.

Declaration of competing interest

The authors declare that they have no known competing financial interests or personal relationships that could have appeared to influence the work reported in this paper.

Acknowledgments

References

[1] L. Ma, T. Zhang, J. Energy Chem. 80 (2023) 48–57.
[2] Y. Chen, Y. Kang, Y. Zhao, L. Wang, J. Liu, Y. Li, Z. Liang, X. He, X. Li, N. Tavajohi, B. Li, J. Energy Chem. 59 (2021) 83–99.
[3] H. Pang, L. Wu, J. Liu, X. Liu, K. Liu, J. Energy Chem. 78 (2023) 1–12.
[4] H. Shi, S. Wang, J. Liang, P. Takyi-aninakwa, J. Energy Chem. 82 (2023) 521–536.
[5] R. Xiong, J. Tian, W. Shen, J. Lu, F. Sun, J. Energy Chem. 76 (2023) 404–413.
[6] K. Luo, X. Chen, H. Zheng, Z. Shi, J. Energy Chem. 74 (2022) 159–173.
[7] X. Li, D. Yu, V. Søren, S. Daniel, J. Energy Chem. 82 (2023) 103–121.
[8] Y. Che, X. Hu, X. Lin, J. Guo, R. Teodorescu, Energy Environ. Sci. (2023) 338–371.
[9] X. Chen, J. Choi, X. Li, ACS Energy Lett. 7 (2022) 4362–4367.
[10] X. Liu, X.Q. Zhang, X. Chen, G.L. Zhu, C. Yan, J.Q. Huang, H.J. Peng, J. Energy Chem. 68 (2022) 548–555.
[11] Y. Che, D.I. Stroe, X. Hu, R. Teodorescu, IEEE Trans. Ind. Informatics 19 (2023) 6471–6481.
[12] X. Sui, S. He, J. Meng, R. Teodorescu, D.I. Stroe, IEEE J. Emerg. Sel. Top. Power Electron. 9 (2021) 5125–5137.
[13] X. Li, C. Yuan, Z. Wang, J. Xie, Energy 239 (2022).
[14] Y. Che, S.B. Vilsen, J. Meng, X. Sui, R. Teodorescu, ETransportation 17 (2023).
[15] X. Liu, H. Peng, B. Li, X. Chen, Z. Li, J. Huang, Q. Zhang, Angew. Chemie 134 (2022) e202214037.
[16] S. Greenbank, D. Howey, IEEE Trans. Ind. Informatics 18 (2022) 2965–2973.
[17] Q. Gong, P. Wang, Z. Cheng, J. Energy Storage 46 (2022).
[18] H. Ruan, J. Chen, W. Ai, B. Wu, Energy AI 9 (2022).
[19] K.A. Severson, P.M. Attia, N. Jin, N. Perkins, B. Jiang, Z. Yang, M.H. Chen, M. Aykol, P.K. Herring, D. Fraggedakis, M.Z. Bazant, S.J. Harris, W.C. Chueh, R.D. Braatz, Nat. Energy 4 (2019) 383–391.
[20] S. Ji, J. Zhu, Z. Lyu, H. You, Y. Zhou, L. Gu, J. Qu, Z. Xia, Z. Zhang, H. Dai, J. Energy Chem. 78 (2023) 565–573.
[21] X. Tang, F. Gao, X. Lai, ETransportation 13 (2022).
[22] Y. Tan, G. Zhao, IEEE Trans. Ind. Electron. 67 (2020) 8723–8731.
[23] S. Panigrahi, A. Nanda, T. Swarnkar, Smart Innov. Syst. Technol. 194 (2021) 781–789.
[24] C. Bian, S. Yang, Q. Miao, IEEE Trans. Transp. Electrif. 7 (2021) 1260–1270.
[25] T. Han, Z. Wang, H. Meng, J. Power Sources 520 (2022).
[26] Y. Che, Y. Zheng, Y. Wu, X. Sui, P. Bharadwaj, D. Stroe, Y. Yang, X. Hu, R. Teodorescu, Appl. Energy 323 (2022).
[27] X. Liu, F. Zhang, Z. Hou, L. Mian, Z. Wang, J. Zhang, J. Tang, IEEE Trans. Knowl. Data Eng. 35 (2021) 857–876.
[28] M. Noroozi, A. Vinjimoor, P. Favaro, H. Pirsiavash, Proc. IEEE Comput. Soc. Conf. Comput. Vis. Pattern Recognit. (2018) 9359–9367.
[29] W.J. Murdoch, C. Singh, K. Kumbier, R. Abbasi-Asl, B. Yu, Proc. Natl. Acad. Sci. U. S. A. 116 (2019) 22071–22080.
[30] R. Xiong, Y. Sun, C. Wang, J. Tian, X. Chen, H. Li, Q. Zhang, Energy Storage Mater. 57 (2023) 460–470.
[31] J. Zhu, Y. Wang, Y. Huang, R. Bhushan Gopaluni, Y. Cao, M. Heere, M.J. Mühlbauer, L. Mereacre, H. Dai, X. Liu, A. Senyshyn, X. Wei, M. Knapp, H. Ehrenberg, Nat. Commun. 13 (2022) 1–10.
[32] K. Liu, Q. Peng, Y. Che, Y. Zheng, K. Li, R. Teodorescu, D. Widanage, A. Barai, Adv. Appl. Energy 9 (2023).
[33] J. Guo, Y. Che, K. Pedersen, D.-I. Stroe, J. Energy Chem. 79 (2023) 211–221.